PAPER

Check for updates

Effects of plasma activated water on fava bean protein isolate functionality and 3D printability

Pauline Chan, [ID] [a] Sitian Zhang,[a] Anuruddika Hetti Hewage,[b] Shifa Dinesh,[a] Nandika Bandara, [ID] [b] Thava Vasanthan,[a] Lingyun Chen,[a] N. N. Misra[c] and M. S. Roopesh [ID] *[a]

Fava bean protein is an emerging food ingredient with many health benefits and great potential in the plant-based meat industry. However, fava bean proteins often have inferior functionality, such as poor solubility compared to animal proteins. Therefore, it is pertinent to explore methods of protein modification that target improving protein functionality for commercial applications. Cold plasma is a novel non-thermal green technology that ionizes gas molecules to produce reactive species that can chemically interact with proteins. This study explores the effects of plasma activated water (PAW) on fava bean protein isolates (FBPI). Using a jet plasma system, PAW was produced from a mixture of argon gas and air. The PAW was then subsequently mixed with fava bean protein isolates to produce thermally set gels. FBPI treated with PAW demonstrated changes in secondary structures, with conversion from α-helices to β-sheets. Treated FBPI gels also exhibited increases in gel strength and improved 3D printability. Gel color, and gel adhesion also demonstrated some changes after PAW treatment in some conditions. Overall, PAW treatment was demonstrated to be a mild method for FBPI modification.

Sustainability spotlight

This research can be utilized to enhance current practices in protein modification within the food industry, leading to greener and milder modification techniques. Additionally, 3D printing of plant proteins is a novel technology that can be utilized for both industrial and consumer applications.

1. Introduction

Fava bean proteins have been gaining interest in both industry and research due to their high protein content and functionality. Previous research focused on evaluating the use of FBPI as a main ingredient in meat alternatives due to their similarity to meat texture.[1] However, the challenge when working with pulse proteins such as FBPI is their hydrophobicity, high aggregation and low solubility.[2] Comparing protein functionalities, animal proteins are generally regarded as far superior to plant proteins, especially regarding gelling, foaming and emulsifying abilities.[3] Therefore, modification of plant proteins is required to facilitate the adoption of plant proteins as animal protein alternatives in food applications. Currently, the industry employs various methods to modify plant proteins, such as pH shifting, thermal treatment or enzymatic modification. These methods involve using strong bases and acids, which can be environmentally detrimental and costly. Thermal treatments, while effective, are energy-intensive and expensive. This demands the development of sustainable technologies to modify plant proteins for industrial adoption. Cold plasma is one such technology that could bridge these gaps.

Plasma is commonly referred to as the fourth state of matter and is composed of highly reactive and ionized particles. Typically, ionizing particles past the gas phase require significant heat and energy; however, generating cold plasma is another option. Cold plasma or non-thermal plasma can be produced at room temperature and atmospheric pressure *via* strong electric fields to ionize gas particles. Introduction of ionized gas into water results in the formation of solvated reactive species, resulting in the formation of Plasma Activated Water (PAW). Among the many available design configurations, to produce plasma activated water (PAW), a jet reactor or bubble reactor can be used.[4] Herein, air and/or inert gases such as argon are directed into the reactor, where it is exposed to strong electric fields, causing partial ionization. The ionization results in the formation of reactive oxygen and nitrogen species (RONS). Subsequently, the ionized gas mixture is then expelled directly into water, creating PAW. It is worth mentioning that plasma

[a]*Department of Agricultural, Food & Nutritional Science, University of Alberta, Edmonton, Alberta, Canada. E-mail: roopeshms@ualberta.ca*

[b]*Department of Food and Human Nutritional Sciences, University of Manitoba, Winnipeg, Manitoba, Canada*

[c]*Department of Clinical Laboratory Sciences, College of Applied Medical Sciences, Taif University, Taif, Saudi Arabia*

chemistry is governed by the process parameters such as various gas feeds, ratios, flow rates, voltages and frequency. Different parameters result in different conditions, all of which can affect the samples differently.

Cold plasma from dielectric barrier discharge (DBD) systems has been previously investigated for plant protein modification, with pea protein being the most common.[5–7] PAW was also utilized to successfully modify myofibrillar proteins, as well as pea protein modification.[5,8] However, as of currently, no studies have explored the use of PAW for fava bean protein. Structural modifications of proteins are often attributed to the reactive species in PAW that interact *via* hydrogen bonding and disulfide linkages.

Menon *et al.* (2024) explored optimized PAW gas ratios for the improvement of the 3D printability of pea proteins.[5] Similar procedures and methods were adopted in this current study with FBPI. Compared to peas, fava beans generally contain higher protein content. Asledottir *et al.* (2023) reported peas containing 56.2% (dry matter) protein and fava beans containing 63.2% (dry matter) protein.[9] The higher protein yield may be a desirable and economical option for producers, which reinforces the need to expand research for FBPI utilization and processing.

With PAW treatments, it was hypothesized that the ROS and RNS in the PAW will be sufficient in inducing structural modifications that can improve FBPI functionality, such as solubility, 3D printability and rheological properties. The main objective of this study is to utilize PAW to induce structural modifications in sustainably extracted fava bean protein isolates and to analyze the modified characteristics.

2. Materials and methods

2.1 Materials

Two different sources of FBPI were used in this study. The dry and wet FBPI (DW-FBPI) was sourced from a local company in Edmonton, AB, Canada. DW-FBPI was extracted by a patented technology incorporating vacuum, high-pressure air and a sieve combined with aqueous fractionation.[10,11] The second type of FBPI was obtained using deep eutectic solvent extraction (DES), as outlined by Hewage *et al.* (2024) with slight modifications.[12] In brief, fava bean flour was mixed with 50% DES containing choline chloride and glycerol (1 : 2 molar ratio w/w) and 50% water (w/w) at a 12.5 : 1 liquid-to-solid ratio. It was then homogenized at a speed of 20 000 rpm for 2 min (Model 850, Fisher Scientific, Ottawa, ON, Canada), followed by protein extraction using a circulating water bath (Model 6200 H7, Fisher Scientific Inc, Pittsburgh, PA, USA) at 200 rpm, 50 °C for 1 h. The supernatant collected after centrifugation ($17\,709 \times g$, 10 min, 4 °C) was dialyzed (3.5 kDa) at 4 °C for 5 days, with continuous refreshment with distilled water. Finally, the resulting protein solution was freeze-dried and stored at −20 °C. The dried protein obtained was referred to as deep eutectic solvent extracted fava bean protein isolates (DES-FBPI).

MilliQ water (Direct-Q™ 3 Tap, MilliporeSigma, Burlington, USA) was used for PAW as well as the main solvent in control

samples. Sodium hydroxide used in pH shifting of DES-FBPI samples was obtained from Sigma-Aldrich (St. Louis, MO, USA).

2.2 Methodology

2.2.1 Protein content. Crude protein was measured using the Flash 2000 Organic Elemental Analyzer (Thermo Fisher, Waltham, MA, USA). Untreated samples were used in protein content measurement, and a conversion factor of 6.25 was used to calculate protein content.[13] Additional protein content calculation corrections were conducted using a conversion factor of 5.4.[14] Untreated samples were used for protein analysis to understand the protein purity of the FBPI. Using tin capsules, 5 mg of the samples were deposited and sealed before analysis. Samples were measured in triplicate, and the final data were obtained by averaging the values.

2.3 Plasma jet system

The plasma jet reactor was supplied by Ingenium Naturae Pvt Ltd, Mumbai, India. Fig. 1 illustrates the system set-up alongside the power supply (PG 100-3D, Advanced Plasma Solutions, Malvern, USA). The gas dispersion frit was custom-made at the University of Alberta glass shop, featuring a Type C frit size with pores ranging from 25–50 μm. To accommodate the custom glass frit, a brass full-flow quick-connect fitting was obtained from Swagelok, Edmonton, AB, Canada. The power supply system was operated at a frequency of 3500 Hz, a duty cycle of 70 and an average voltage of 30 kV. Using a gas flow controller, a mixture of argon (1.8 L min^{-1}) and air (0.2 L min^{-1}) with a ratio of 90 : 10 was used for plasma production in the plasma jet system (Whisper™ MW series Meters, Alicat Scientific, Tucson, USA).

2.3.1 Optical emission spectra. Optical emission spectroscopy (OES) is a real-time technique that analyzes the light emitted from plasma to identify the reactive species based on electronic transitions. The optical emission spectra were obtained using a spectrophotometer (Black Comet, C-25, S/N 17060712, StellarNet Inc., Tampa, FL, USA) with a resolution of 0.5 nm, in a wavelength region from 180 to 850 nm and an optical fiber (F600-UVVIS-SR, StellarNet, Inc., Tampa, FL, USA). To acquire a spectrum, the optical fiber was focused on an unobstructed section of the plasma reactor, 1 cm away from the reactor walls. A black cloth was used to obstruct stray light, and measurements were recorded once peaks reached a maximum. Data from the OES was captured and analyzed using the SpectraWiz Software (StellarNet, Inc., Tampa, FL).

2.3.2 Plasma activated water characterization. Various characteristics of PAW were measured and analyzed, including pH, oxidation–reduction potential (ORP), conductivity, and reactive species content. Reactive species measurements were detected using chemical kits and a V-2000 Multi-analyte photometer (CHEMetrics, Calverton, VA, USA). This study utilized ozone K7404, hydrogen peroxide K-5543 and nitrite K-7004C CHEMmet® kits. The procedure was followed based on the manufacturer's methods.

2.3.2.1 Ozone. Ozone CHEMmets® kits employ DPD (*N*,*N*-diethyl-*p*-phenylenediamine) chemistry to evaluate ozone
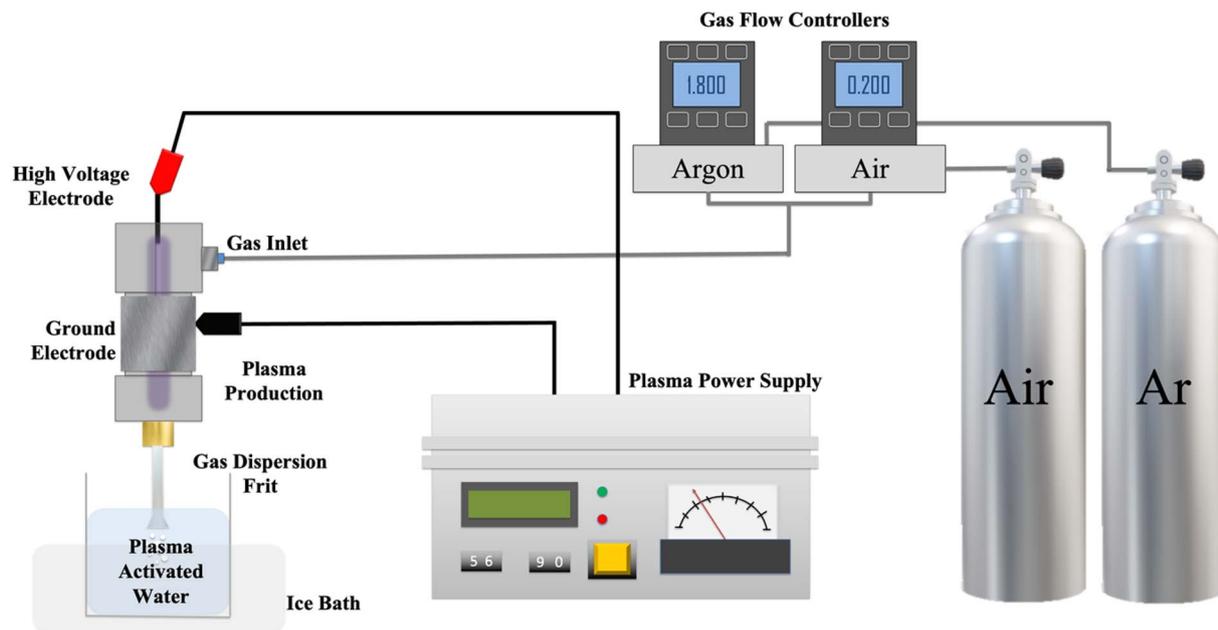
Fig. 1 Jet plasma system used in this study.

content. The sample is first treated with excess potassium iodide. Ozone present in the sample oxidizes iodide into iodine. Subsequently, iodine then oxidizes DPD (*N,N*-diethyl-*p*-phenylenediamine) to form a pink color, which is directly proportional to the ozone concentration present in the sample.

2.3.2.2 Hydrogen peroxide. Hydrogen peroxide CHEMmets® kits utilize ferric thiocyanate chemistry. In acidic environments, hydrogen peroxide oxidizes ferrous iron. The remaining ferric iron then reacts with ammonium thiocyanate to form ferric thiocyanate, creating a red/orange color complex which is directly proportional to the hydrogen peroxide content in the sample.

2.3.2.3 Nitrite. Nitrite CHEMets® test kits utilize the azo dye formation method. In acidic environments, nitrite diazotizes with primary aromatic amine and couples with another organic molecule to produce azo dye. The result is a pink-orange color, the intensity of which is proportional to the nitrite concentration in the sample.

2.3.3 Oxidation–Reduction potential (ORP). The oxidation–reduction potential of PAW samples was estimated to identify the oxidizing or reducing capacity of PAW. Using a portable ORP pen meter (ST20R, Ohaus, Parsippany, USA), the probe was placed in the sample for 1 min, allowing for readings to stabilize before being recorded.

2.4 Preparation of PAW and FBPI suspension

Before plasma generation, the plasma jet system was primed with 2 L min^{-1} of a 90 : 10 Ar : Air gas mixture prepared with a gas flow controller (Whisper™ MW series Meters, Alicat Scientific, Tucson, USA). An ice water bath was prepared for the sample beaker, which contained 100 mL of MilliQ water. For PAW generation, the end of the glass frit was positioned 0.5 cm from the bottom of the beaker. Power was turned on, and PAW

was generated for 30 min for DW-FBPI and 8 min for DES-FBPI. The 30 min treatment time was based on Menon *et al.* (2024) study on optimized PAW treatment for pea proteins, whereas the 8 min treatment time was based on trials conducted for FBPI.[5]

For the DW-FBPI suspension, 20 g of DW-FBPI was deposited in a 250 mL glass beaker. Eighty milliliters of PAW were added to DW-FBPI to create a 20% w/w solids concentration. The samples were manually mixed for 1 min with a metal spatula and subsequently magnetically stirred for 1 h at 350 rpm. After the first mixing cycle, pH and viscosity measurements were taken. The second mixing cycle was completed at 4 °C for 1 h with a 250 rpm magnetic stirring speed.

For DES-FBPI suspension, pH shifting was required as the pH of the protein solution was near its isoelectric point, which hindered the solubility. Approximately 1000 μL of 5 M NaOH was used to shift the protein solution to a pH of 7. In addition, DES-FBPI suspensions were mixed with PAW generated with 8 min of plasma treatment. The pH shifting was conducted after the second round of mixing at 250 rpm, 4 °C for 1 h. Two additional rounds of refrigerated stirring were completed after pH shifting.

As the preparation procedures for DES-FBPI and DW-FBPI are different, they were completed independently and not compared. The FBPI suspensions prepared using PAW were named "treated" and the FBPI prepared using MilliQ water was named "control" in this paper.

2.5 Pre-gelation FBPI characterization

Pre-gelation FBPI characterization was completed before protein suspensions underwent heat-induced gelation.

2.5.1 pH measurement. An Accumet Basic AB15 pH meter (Thermo Fisher, Waltham, MA, USA) was used to obtain pH

readings. The pH was measured at room temperature and readings were recorded after one minute to allow the values to stabilize.

2.5.2 Solubility. The FBPI solubility method was adapted from methods described by Yang *et al.* (2019).[16] All treated and control FBPI suspensions were centrifuged at $4000 \times g$ for 30 min at room temperature in a 50 mL Falcon tube. After centrifugation, the supernatant and residual pellets were separated and frozen in a −12 °C freezer for a minimum of 48 h. The sample tubes were then freeze-dried for 72 h. Initial and final weights were recorded. The solubility (%) was calculated from the following modified equation:

$$\text{Solubility} = \frac{W_1}{(W_1 + W_2)} \times 100\% \tag{1}$$

where W_1 is the freeze-dried supernatant weight and W_2 is the freeze-dried precipitate weight.

2.5.3 Conductivity. Using the 4360 Traceable Expanded Range Conductivity Meter (Traceable Products, Houston, USA), readings were obtained for PAW and the FBPI suspensions. Data was recorded approximately one minute after the conductivity probe was submerged in the samples to allow the readings to stabilize. When the probe displayed "ready" the readings were recorded.

2.5.4 Viscosity. The FBPI samples were evaluated using a Fungilab Viscobasic Plus Viscometer (Fungilab, Hauppauge, NY). Samples were dispensed into a 150 mL beaker and filled to 50 mL. To ensure accuracy of viscosity measurements, residual foam was removed with a spatula. An R2 spindle with a maximum spindle speed of 100 rpm was used. After readings stabilized, viscosity measurements were recorded. All viscosity analyses were completed at room temperature.

2.5.5 Zeta potential. For zeta potential determination of the FBPI samples, a Zetasizer Nano-ZS (Malvern Instruments Ltd, UK) was used. Specifications for the analysis included a protein refractive index (RI) of 1.45 and dispersion medium RI of 1.33.[6] The protein samples were diluted to a final concentration of 1 mg mL^{-1} with MilliQ water. Before analysis, samples were kept under refrigeration at 4 °C.

2.5.6 Circular dichroism (CD). Circular dichroism (CD) is a useful analytical technique that evaluates the chirality of molecular systems and can be used to characterize secondary structures in proteins by comparing existing standards.[17] For CD analysis measurements, only the soluble fractions of the fava bean protein samples were used. Treated and controlled FBPI suspensions were centrifuged at $4000 \times g$ for 30 min to separate the supernatant and precipitate. After separation, the samples were frozen completely in a −21 °C freezer and freeze-dried to remove moisture. The supernatant fraction was then crushed into a fine powder and dissolved in a $1 \times$ phosphate buffered saline (PBS) pH 7.4 buffer with a final concentration of 1 mg mL^{-1}. The protein buffer solution was then filtered with a 0.22 μm filter. The CD analysis of the resulting FBPI solutions was performed using the Olis 1 instrument and OLIS Globalworks software (On-Line Instrument Systems Inc., Athens, GA, USA) at the Department of Chemistry, University of Alberta. Calculations were based on buffer subtraction and a digital 13

filter for smoothing. Finally, the data were converted to molar ellipticity. The samples were formulated at a concentration of 1 mg mL^{-1}/AA-1097, and a cell path length of 0.02 cm, with recorded spectral length from 190 to 260 nm. Analyses were conducted at a temperature of 25 °C with a fixed bandwidth of 1 nm.

Using an online software BeStSel (Beta Structure Selection) (BeStSelTM ELTE Eötvös Loránd University, Budapest, Hungary), the secondary structure can be determined with CD data.

2.5.7 Fourier transform infrared spectroscopy (FTIR). The FTIR spectroscopy was used to identify chemical bond changes in the FBPI. The FBPI samples were analyzed in a powder form at the Lipids Utilization Lab at the University of Alberta, and analyses were conducted using the Bruker Compact FT-IR Spectrometer ALPHA (Bruker, Billerica, MA, USA). Spectral scans were obtained in the range of 4000 to 400 cm^{-1} at a resolution of 2 cm^{-1}.

2.6 Post-gelation FBPI characterization

After plasma treatment, a portion of the FBPI samples was heated in a water bath for 30 min to 1 h at various temperatures (95, 85, 80, and 79 °C) to induce gelation. Gel characteristics were studied in this section to understand the effects of plasma treatment on FBPI gelation and related properties.

2.6.1 Colorimetry. Color was measured for FBPI gels using a CR-400 Colorimeter at a 2° observer angle and illuminated by a pulsed xenon lamp (Konica Minolta, Mississauga, ON). Gels were deposited on a tin pan and smoothed out. To measure, the colorimeter was positioned directly above the gel samples, ensuring the sample fully covered the light projection tube opening. The colorimeter was set to take 3 measurements, and the average was recorded. Colorimetry data were recorded in the CIE $L^*a^*b^*$ or CIELAB 2000 color space. The parameter L^* indicates lightness (+) and darkness (−) from 0 to 100, respectively. The a^* parameter measures redness (+) and greenness (−), whereas the b^* parameter measures yellowness (+) and greenness (−). The values close to zero for the a^* and b^* parameters indicate they are neither positive nor negative color. The final parameter that can be retrieved from colorimetry data is the ΔE value. This is a calculated value that measures how different two colors are in the CIE LAB color space.

$$\Delta E = \sqrt{(L_t - L_c)^2 + (a_t - a_c)^2 + (b_t - b_c)^2} \tag{2}$$

where t indicates treated and c indicates control.

2.6.2 Water holding capacity (WHC). The FBPI gel's water holding capacity was measured by methods described in Zhang *et al.* (2022) with modifications.[7] Approximately 0.5 g of the FBPI gels was loaded into a 1.5 mL microcentrifuge tube and centrifuged at $4000g$ for 30 min. After centrifugation, the expelled water was removed, and the final weight of the gel was obtained. To calculate the WHC, the following equation was used

$$\text{WHC} = \frac{W_1 - W_2}{W_1} \times 100\% \tag{3}$$

where W_1 is the total weight of the gel before centrifugation, and W_2 is the weight of the expelled water from the gel due to centrifugation.

2.6.3 3D printability. Sample tubes containing FBPI samples were heated in a hot water bath (Fischer Scientific, Waltham, Massachusetts, USA) at temperatures ranging from 79 to 95 °C for 30 min or 1 h. After heat treatment, tubes were moved to an ice water bath to cool for 1 h. Before 3D printing, tubes were returned to room temperature. The 3D printing of FBPI gels was completed on the FoodBot 3D-Printer (Shiyin-Tech, Hangzhou, China). Approximately 15 g of sample was dispensed into 3D printing extrusion tubes. The 3D printed shape design was a cylinder with 30% infill (Menon *et al.*, 2024).

The 3D printability of FBPI gels was evaluated in three ways: photographic data, digital measurements and calculated parameters. Shape measurements provide information regarding the integrity of the shape, specifically the degree of spread experienced by the 3D printed object (Tables S8 and S9).

Photographs were taken once printing was completed and 24 h after printing. The height, length and area of each 3D printed gel were measured and analyzed using ImageJ software (National Institute of Health, Maryland, USA). 3D printer parameters included a travel speed of 15 mm s^{-1}, a bottom layer speed of 15 mm s^{-1}, amount fill of 30%, a retraction speed of 50 mm s^{-1}, a retraction distance of 2 mm, layer height of 0.75 mm, a fill density of 23% and a print speed of 20 mm s^{-1} (Menon *et al.*, 2024).

2.6.4 Texture profile analysis (TPA). The gels were heated in a 10 mL beaker, ensuring uniform diameters. After decanting the gels, they were cut to a height of 1 cm and positioned in the middle of the cylindrical plunger of the texture profile analyzer (Stable Micro Systems, Godalming, UK). For sample analyses, the plunger was set to the top of the gel height at 10 mm. Standard pre-set parameters were used with a 1.0 mm s^{-1} pre-test speed, 2.0 mm s^{-1} test speed, 2.0 mm s^{-1} post-test speed, 5.0 mm distance, 5.0 s time, and 1.0 g of trigger force. The plunger was depressed twice with 50% strain. Three replicates were completed for each sample and averaged.

The texture profile analyzer provides measurements for hardness and calculated values for fracturability, cohesiveness, springiness, gumminess, chewiness and resilience by conducting two compressions on the sample. Not all the calculated values are relevant to the nature of the sample; therefore, some parameters were omitted in the study. The formulae for the calculated parameters are outlined below (Texture Technologies Corp. and Stable Micro Systems, Ltd, Hamilton, MA, USA).

$$\text{Hardness} = \text{peak force at first compression} \quad (4)$$

$$\text{Adhesiveness} = \text{work required for probe to overcome attractive force} \quad (5)$$

$$\text{Cohesiveness} = (\text{area 2/area 1}) \quad (6)$$

$$\text{Springiness} = (\text{distance 2/distance 1}) \quad (7)$$

$$\text{Gumminess} = \text{hardness} \times \text{cohesiveness} \quad (8)$$

For cohesiveness, area 1 is the area under the first compression of the TPA curve whereas area 2 is the area under the second compression of the TPA curve. For springiness, distance 1 is the time in seconds it takes to reach peak force from 0 g during the first compressions. Distance 2 is the time required to reach peak force from 0 g during the second compression.

2.6.5 Rheology. Amplitude sweep and frequency sweep analyses were conducted using the Anton Paar Physica MCR 301 rheometer (Anton Paar, Graz, Austria). For analysis preparation, FBPI suspensions were heated in a water bath at various temperatures (79, 80, 85 and 95 °C) for 30 or 60 min in a 10 mL beaker. After gelation, the samples were trimmed to a height of 5 mm. All samples were analyzed at a temperature of 20 °C. For the amplitude sweep, samples were analyzed with an initial strain of 0.01% and a final strain of 100%. The angular frequency was set to 10 s^{-1}. The linear viscoelastic range (LVE) was auto calculated in the Rheoplus software (Anton Paar, Graz, Austria) using an equipment standard of 5% smoothing range and a 10% tolerance band. Once the appropriate strain% was identified from the amplitude sweep, it was utilized in the frequency sweep. All analyses were conducted with a 25 mm diameter parallel plate spindle. In frequency sweep analysis, the storage modulus (G') and the loss modulus (G'') are values converted from torque measurements, which are the resistance inflicted by the sample on the testing spindle at a set speed. The frequency sweep data were originally recorded in Pa (shear stress) against Hz (frequency), but were later converted into angular frequency rad s^{-1} for further calculations and statistical analysis. All samples were analyzed in three replicates and averaged.

2.7 Statistical analysis

Experiments were conducted in triplicate with data statistically analyzed using the software, Origin (Origin 2024 Home-Use edition, OriginLab Corporation, Northampton, MA). One-way and two-way ANOVA tests were conducted, where appropriate, with Tukey's test as *post hoc* analysis to identify any significant differences present between sample groups ($P < 0.05$).

3. Results and discussion

3.1 Protein content

Two different protein content values were obtained for each FBPI sample. DW-FBPI had a measured protein content of $86.02 \pm 0.62\%$ and a corrected protein content of $74.32 \pm 0.54\%$. DES-FBPI had a measured protein content of $96.61 \pm 1.49\%$ and a corrected protein content of $83.47 \pm 1.29\%$. Obtaining the protein content values provides additional context regarding sample composition. The standard conversion factor 6.25 overestimates the amount of protein present in a sample, hence the justification for correcting to a conversion factor of 5.4. Compared to the DW-FBPI, the DES-FBPI has a higher protein content. The higher protein content in DES-FBPI compared to DW-FBPI aligns with its higher solubility (discussed later in Section 3.5), likely due to the deep eutectic solvent extraction
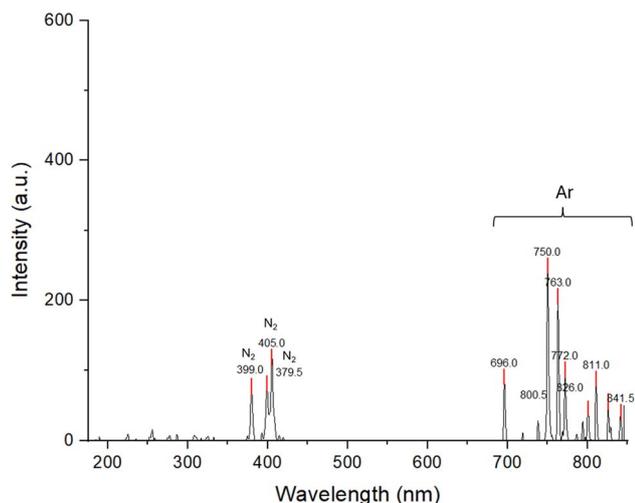
Fig. 2 Optical emission spectrum of the plasma jet with 90 : 10 Ar : Air gas feed.

method, which may enhance protein purity by reducing non-protein components.[12]

3.2 Optical emission spectra (OES)

Prominent peaks in emission spectra were compared with previous literature as well as Ver 5.12 NIST Atomic Spectra Database for identification.[18,19] A total of 11 peaks (Fig. 2) were identified from the OES spectrum, including peaks for Ar (696, 750, 763, 772, 800, 811, 826, 841 nm), and N_2 (around 399 nm and 379 nm) (Table S1). The majority of the peaks were detected in the visible wavelength (400 to 800 nm), and several minor peaks were in the UV range (200 to 400 nm) (Table S1). Previous studies exploring jet plasma produced from argon observed similar findings.[20,21]

3.3 PAW characterization

During PAW production, certain attributes of water can change. Evaluating these attributes indicates whether the plasma treatment was effective. Table 1 demonstrates significant differences in pH, ORP, and conductivity. Plasma treatment induced acidification in the PAW, reducing the pH of MilliQ water from a pH of 6.09 to a pH of 4.15. As for the oxidizing ability, PAW had a 100 mV increase compared to untreated MilliQ water. Conductivity also increased significantly from 0.9 μS to 36.93 μS after plasma treatment. Increases in conductivity in the PAW can be attributed to the presence of the reactive ions

in Table 1. After plasma treatment, PAW demonstrated an increase in ozone, H_2O_2, and nitrite.

Previously, Menon *et al.* (2024) also explored PAW production with a 90 : 10 Ar : Air ratio.[5] However, the reported ORP, conductivity, and RONS values in PAW in this study (Table 3) are relatively lower, possibly due to the different types of reactor and process parameters used in this study.

3.4 pH measurements

3.4.1 DW-FBPI. The initial pH of the PAW was 4.37 ± 0.11. After mixing DW-FBPI with PAW, the pH shifted to 6.55 ± 0.07. Control samples had a pH of 6.47 ± 0.05. Immediately after mixing, the treated samples had a more basic pH compared to the control samples. However, after all the mixing cycles, the final pH of the treated samples (6.47 ± 0.04) was not significantly different from the control (6.45 ± 0.03). Due to proteins containing positively charged amino groups as well as negatively charged carboxyl groups, it is possible that the DW-FBPI acted as a buffer and resisted changes in pH despite the acidic conditions of PAW.

3.4.2 DES-FBPI. DES-FBPI was tested with two different conditions, *i.e.*, 8 min PAW generation and 30 min PAW generation. As pH shifting is necessary for DES-FBPI, measurements were taken both before and after the pH adjustment to evaluate the effects of PAW on pH. Despite a significant difference ($P < 0.05$) in pH between MilliQ water and PAW, there were no changes observed once combined with DES-FBPI for both the 8 min PAW and 30 min PAW. The protein suspension's initial pH was around 5.25, and the final pH was around 6.92 for both treated and control samples.

According to Luo *et al.* (2018), side groups, *viz.*, aspartic acid (Asp), glutamic acid (Glu) and the terminal carboxyl group, are effective buffering components.[22] DES-FBPI contains relatively high amounts of Asp (9.3 g/100 g DES-FBPI) and Glu (14.4 g/100 g DES-FBPI), which possibly may have contributed to the buffering effects observed.

3.5 Solubility

The solubility values of DW-FBPI for both treated and control samples were around 42.6% with no significant difference ($P > 0.05$). A similar result was observed for DES-FBPI samples, with solubility values for both treated and control samples was around 69.4%. Compared to DW-FBPI, DES-FBPI had higher solubility. Based on the solubility results, the PAW treatments were not effective in improving the solubility of FBPI. These results do not agree with previous studies in which improved solubility was observed for PAW treated whey protein isolate.[23] Ji

Table 1 Characterization parameters and reactive species detected in jet plasma activated water[a]

	pH	ORP (mV)	Conductivity (μS)	Ozone (mg L⁻¹)	Hydrogen peroxide (mg L⁻¹)	Nitrite (mg L⁻¹)
MilliQ water	6.09 ± 0.20[a]	285 ± 22[a]	0.90 ± 0.09[a]	0.000 ± 0.000[a]	0.012 ± 0.020[a]	0.021 ± 0.001[a]
PAW	4.15 ± 0.07[b]	385 ± 7[b]	36.93 ± 3.49[b]	0.150 ± 0.022[b]	0.132 ± 0.025[b]	0.036 ± 0.005[b]

[a] Values are expressed as the mean ± the standard deviation of three replicates. 1-way ANOVA was completed with Tukey test as *post hoc* test. The alphabetical superscript (a, b) indicates the values that are significantly different between MilliQ water and PAW ($p < 0.05$).

et al. (2018) also reported improvements in solubility after dielectric barrier discharge plasma treatment of peanut protein isolates.[24] According to previous studies of PAW-treated Bambara groundnut globulin, another plant protein, the PAW exposed polar amino acids buried within the protein, ultimately increasing hydrophilicity on the surface and improving solubility.[25] The solubility results from this study suggest that the protein unfolding by PAW was insufficient for solubility improvements. More intensive PAW treatments may be required to improve solubility in FBPI.

3.6 Conductivity

Conductivity analysis was performed only for the DES-FBPI suspensions due to sample limitations. The conductivity of treated samples was 1884.7 ± 237.0 µS, whereas that for the control samples was 1937.7 ± 119.3 µS. No significant differences in conductivity values were observed. Although the method of plasma treatments was slightly different, Sun *et al.* (2021) observed increases in conductivity for plasma-jet treated wheat gliadin acidified alcohol suspensions.[26] Major differences in Sun *et al.* (2021) study include the primary use of Helium for plasma generation, which results in different types of reactive species.[26] Chen *et al.* (2020) observed increased conductivity in zein-chitosan suspensions with prolonged DBD plasma exposure.[27] In addition to shorter treatment times of 2 min and treatments with DBD plasma reactor, Chen *et al.* study on zein-chitosan utilized significantly lower plasma generation voltages of 30–50 V.[27] These two studies demonstrate that plasma treatments can increase the conductivity of the samples, but effects may depend on treatment efficiency, sample or treatment parameters. Laurita *et al.* (2015) had observed that increased acidification (lowered pH) also resulted in increased conductivity in the PAW.[28] The lack of change in conductivity for the DES-FBPI can be correlated with the minimal acidification that was observed in Section 3.4. As pH deviates from neutral pH, more ions are present regardless of acidic or basic conditions. Increased ions result in increased conductivity hence pH changes in a solution can result in increased conductivity.

3.7 Viscosity

Measuring viscosity was slightly challenging as it was observed to change based on the length of stirring time. Viscosity measurements at the beginning of the stir cycle deviated from the viscosity measurements at the end of the stir cycle. Prolonged stirring resulted in lower viscosity suspensions. Referring to Table 2 for DW-FBPI samples, no significant differences were observed ($P > 0.05$). Treated sample viscosities remained relatively stationary after 1 h and 3 h of stirring compared to the control samples. Similarly, DES-FBPI samples also demonstrated no significant differences ($P > 0.05$) between treated and control viscosities.

Some interesting observations include noticeable resistance during manual mixing of DW-FBPI and PAW immediately after combining. This observation was also detailed in Menon *et al.*, (2024) in their study on PAW and pea protein.[5] Viscosity was visibly increased initially after stirring, suggesting protein aggregation; however, upon measurement, no significant differences were observed in the study.[5] Chen *et al.* (2023) explain that strong protein–protein interactions were initially developed, but prolonged stirring cleaved these interactions and decreased the viscosity.[29] PAW treatments appear to have limited effects on protein viscosity. However, another study investigating DBD plasma treated pea proteins reported increased viscosity after plasma treatment, citing aggregation and crosslinking as the reasons.[7] Different modes of plasma generation, such as DBD plasma systems, may be required to increase viscosity.

3.8 Zeta potential

To measure electrochemical equilibrium at the particle liquid interface, a zeta potential analysis was performed. Analyzing the zeta potential of a sample solution provides insights into the suspension stability.[30] Zeta potential measurements were only obtained for DES-FBPI samples due to sample limitations. No significant differences ($P > 0.05$) in zeta potential of the treated DES-FBPI samples and the control samples were observed. Parameters such as pH can influence the zeta potential, as shown in Berg *et al.*' (2009) study exploring changing pH and nanoparticle suspensions.[31] As pH approaches the isoelectric point of the suspended particles, the zeta potential shifts towards 0, which encourages agglomeration of particles due to the neutral charge at the liquid interface. In Section 3.4, limited pH changes were observed between control and treated samples; therefore, zeta potential values were not expected to deviate either.

According to a technical note published by Malvern (2015), suspensions with a zeta potential between -30 and $+30$ mV are deemed unstable as the surface charge is not significant enough to repel the particles from agglomerating.[15] Therefore, it can be concluded that the application of PAW did not significantly worsen or improve the stability of the DES-FBPI suspension. Another study involving DBD plasma with sunflower seed protein observed changes in zeta potential with prolonged plasma exposure.[32] The zeta potential of the treated sunflower seed proteins reached a maximum after 2 min of treatment, then promptly decreased after 5 minutes of treatment.[32] Based on studies by Zhang *et al.* (2021) and Wang *et al.* (2023), cold plasma appears to impact the suspension stability; however, the

Table 2 Viscosity of DW-FBPI and DES FBPI suspensions[a]

Sample	Time of measurement	Viscosity, v (cP) Control	Treated
DW-FBPI	After 1 h stirring	152.7 ± 9.4^a	157.1 ± 10.9^a
DW-FBPI	After 3 h stirring	152.0 ± 11.0^a	149.6 ± 12.8^a
DES-FBPI	After 30 min PAW generation	125.8 ± 26.8^a	117.8 ± 19.1^a

[a] Values are expressed as the mean $\pm$ the standard deviation of three replicates. 1-way ANOVA was completed with the Tukey test as *post hoc* test. The alphabetical superscript (a, b) within each row and section indicates the values that are significantly different between control and treated ($p < 0.05$).

Table 3 Zeta potential values of DES-FBPI suspensions[a]

PAW generation time	Zeta potential (mV)	
	Control	Treated
30 min	−23.9 ± 1.1[a,A]	−24.0 ± 1.3[a,A]
8 min	−23.9 ± 0.6[a,A]	−24.1 ± 0.7[a,A]

[a] Values are expressed as the mean ± the standard deviation of three replicates. 1-way ANOVA was completed with the Tukey test as *post hoc* test. The alphabetical superscript (a, b) within each row and section indicates the values that are significantly different between control and treated ($p < 0.05$).

effect is determined by the duration of plasma exposure.[6,32] Excess exposure can lead to aggregation and poor suspension stability. Referring to Table 3, the PAW treatment appears to be insufficient in inducing any suspension stability changes. However, further studies focusing on treatment times can help expand the understanding of how PAW treatments can affect suspension stability.

3.9 Circular dichroism

Circular dichroism is a versatile analytical technique that quantifies chirality in molecular systems and is commonly used to identify secondary structures.[17] To extract information from CD spectra, data is compared to known standards for secondary structure calculations.

3.9.1 DW-FBPI. CD analysis was completed before heat treatments were conducted on protein suspensions; therefore, the results represented are induced only by PAW. After mixing with PAW, the helix 1 regular structures in DW-FBPI decreased by 26.5%, but no change in helix 2 distorted secondary structures was recorded (Table 4). The decrease in helix 1 structures was replaced with 26.5% of secondary structures labelled as "others" (Table 4). According to the BeStSel™ CD Data software, the secondary structures allocated as "other" consists of irregular structures and loops. CD data was also visualized in Fig. 3(A). The majority of the curve was relatively overlapped between the treated and control samples, except the 190–195 nm region and the 225–230 nm region. Positive bands in the 190–195 nm and 225–230 nm region indicate helical structures.[33] In Fig. 3(A), treated samples consistently indicated the presence of helical structures, which is also reflected in Table 4.

Table 4 Changes in secondary structure for DW-FBPI and DES-FBPI samples

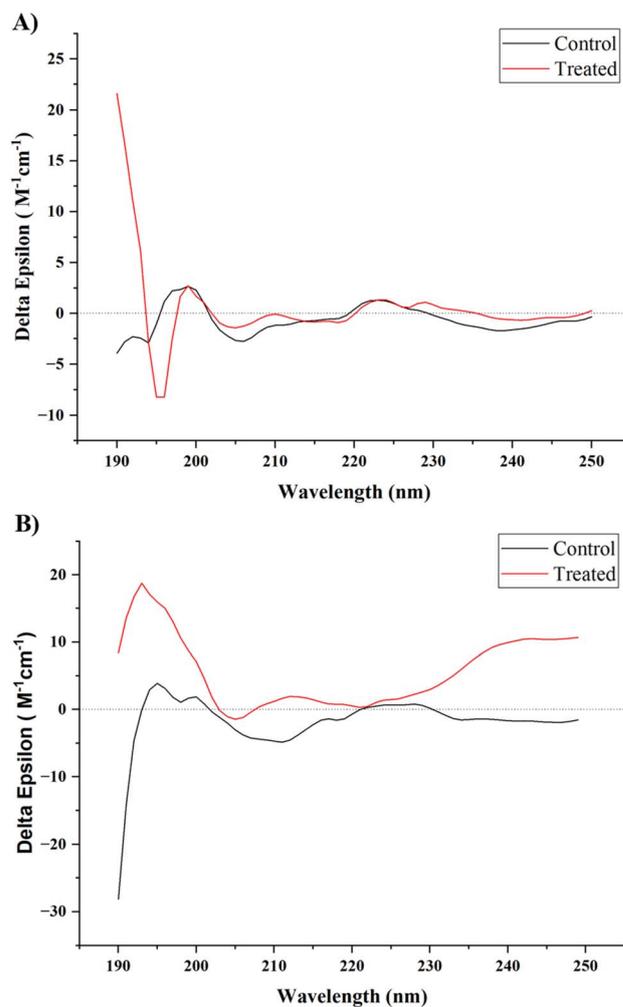|	Secondary structure	Control (%)	Treated (%)
DW-FBPI	Helix 1 (regular)	81.1	54.6
	Helix 2 (distorted)	18.9	18.9
	Others	0.0	26.5
DES-FBPI	Helix 1 (regular)	76.7	0
	Helix 2 (distorted)	11.0	0
	Parallel sheets	12.3	0
	Antiparallel sheets	—	100

Fig. 3 Circular dichroism graph of jet plasma treated DW-FBPI (A) and jet plasma treated DES-FBPI (B).

3.9.2 DES-FBPI. Control DES-FBPI samples demonstrated a variety of secondary structures with mostly helix 1 regular structures (Table 4). After the samples were treated with PAW, the regular helix (76.7%), distorted helix (11.0%), and parallel structures (12.3%) were all converted into anti-parallel β sheet structures. The PAW treatments appear to be very effective in modifying the secondary structures of DES-FBPI. The graphical data in Fig. 3(B) further supports the secondary structural conversions. Fluctuations between negative bands for control samples to positive bands for treated samples are observed in the 190–193 nm, 206–220 nm and 230–250 nm regions. Positive bands in regions 190–193 nm and 230–250 nm represent antiparallel β-sheet structures.[33] Interestingly, the treated samples demonstrated positive bands in regions 206–220 nm, which convey the presence of denatured helical structures; however, these signals were not represented in the calculation from Table 4. A possible explanation for this discrepancy may be the degree of denaturation present in the helical structures; it is possible that they existed as an intermediate between an α-helix and a β-sheet structure, which may have affected the way secondary structures are calculated.

The results for DES-FBPI and DW-FBPI were consistent with previous studies involving plasma treated plant proteins.[24,34] Sharafodin and Soltanizadeh (2022) observed increased β-sheets and random coils in DBD treated soy protein isolates, whereas Ji et al., (2018) observed the same effects in peanut protein isolates after DBD treatment.[24,34] Wang and Damodaran (1991) explained that β-sheet structures in globular proteins are heavily involved in aggregation and network formation in gels.[35] In addition, decreased β-sheets resulted in decreased gel-strength.[35] Observing the conversion of α-helices into parallel and anti-parallel β-sheets signifies that the PAW treatment possibly contributed to improving gel strength.

3.10 FTIR

FTIR analysis was only completed for DW-FBPI samples due to sample limitations. The FTIR spectra indicated the presence of amide I (1636.36 cm^{-1}) and amide II (1518.66 cm^{-1}) (Fig. 4).[36] Minor peaks are observed in the 2800–3600 cm^{-1} region, indicating water and O–H bonds.[37] Another strong peak detected at 1058.41 cm^{-1} is commonly attributed to O–H bonds in carbohydrates.[38] Peak shifting between the treated and control DW-FBPI samples was not present, indicating no changes in molecular bonds or structure. FTIR analysis was initially completed to detect the presence of new bond formations, specifically disulfide bonds. Based on previous studies, plasma treatments were able to increase disulfide bonding, resulting in stronger gel networks (Bahrami et al. 2016; O'Kane et al. 2005).[39,40] Typically, the S–H disulfide stretching frequency appears around 2550 cm^{-1}; however, Fig. 4 did not have any corresponding peaks in that region, indicating limited presence of S–H bonds.[41]

The unchanged molecular bonds suggest that PAW's effects are primarily structural (e.g., β-sheet formation; Section 3.9) rather than covalent. This may limit improvements in gel strength or WHC (as confirmed in Sections 3.12 and 3.14). It is important to note that plasma treatments were completed on the entire FBPI product and not solely on the protein fractions; therefore, interactions with other fractions, such as

carbohydrates or starch, are possible. Future studies could isolate protein fractions or increase plasma intensity to promote disulfide bonding.

3.11 Colorimetry

Significant difference was only detected for L^* (lightness) for DW-FBPI gels heated at 95 °C for 30 min (Table S2). A 7.3% increase in lightness was observed; this is often interpreted as a "bleaching" effect. Overall, the DW-FBPI samples after heat gelation were neither red nor green as their a^* values were relatively close to zero. The samples displayed a more yellow color as they had positive b^* values. The increase in L^* may be attributed to the H_2O_2 reactive species present in PAW, as H_2O_2 is known to be a food-grade bleaching agent.[42] Mahdavian Mehr and Koocheki (2023) observed increased L^* in pea protein isolates after a H_2O_2 control treatment, which partially supports the observations in this study, as PAW contains H_2O_2.[43]

The ΔE values provide information on color differences. The lower the ΔE values, the more challenging it is for the human eye to detect color changes. Apart from the DW-FBPI gels heated at 95 °C for 30 min, most of the shades between the control and treated samples were very difficult to discern (Table S3). Gels heated at 95 °C for 30 min present the highest ΔE value, indicating a larger color difference.

For DES-FBPI gels, a significant difference was observed only for gels heated at 80 °C for one hour (Table S4). The b^* parameter of the 80 °C-1 h treated samples decreased 6.8%, translating to a decrease in yellowness on the CIE LAB 2000 spectrum (Table S4). The decrease in yellowness observed for DES-FBPI gels is not consistent with previous studies exploring plasma treated pea proteins, as increases in b^* (yellowness) were observed.[43]

The 80 °C-1 h DES-FBPI gels presented a ΔE value of 2.44 (Table S3). Observing the gel colors, the treated samples appear darker than the control. With respect to the L^* values, the treated samples had a lower mean L^* value, however, it was statistically insignificant ($P > 0.05$). The gels heated at 79 °C presented a ΔE value of 1.73, however, it did not appear to have a large color difference. The ΔE values are consistent with previous studies investigating DBD plasma treated pea proteins; Bußler et al. (2015) did not observe any product color changes recognizable to the human eye.[44]

It is important to consider color variations between replicates, which is characterized by the standard deviations of the individual L^*, a^*, b^* values as well as the ΔE values. In addition, it is important to note that color differentiation based on ΔE values is subjective, as color perception by the human eye is also subjective. This is especially applicable when observing colors with low ΔE values, which is the case within this study.

Overall, PAW treatments have limited effects on the color of DW-FBPI and DES-FBPI gels and did not impart any negative effects on the color of the samples.

3.12 WHC

The ability of a food ingredient to hold water is a crucial factor in food production. With regards to creating plant-based meats, the
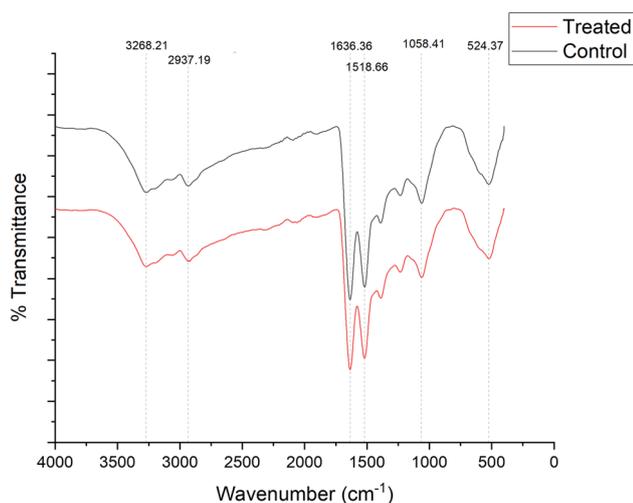

Fig. 4 FTIR spectra of DW-FBPI.

residual water in the protein determines the juiciness of food products.

Comparison of WHC was conducted for different temperatures with similar gelling times such as 1 h or 30 min. The effect of PAW on WHC was insignificant for DW-FBPI gels; however, gelling temperature had a significant effect. Lowering the gelling temperature by 5 °C from 85 °C to 80 °C increased the WHC by approximately 5–8% for DW-FBPI samples (Table S5). For the 30 min gelling time for DW-FBPI samples, a 10 °C decrease in temperature from 95 °C to 85 °C resulted in a 10–12% increase in WHC (Table S5). Gelling temperature appears to be the major determinant of WHC in DW-FBPI gels.

No significant differences in WHC were detected for any of the DES-FBPI gels (Table S5). The unique aspect of DES-FBPI is that it has a high-water holding capacity even without PAW treatment. The WHC of the untreated proteins remains around 98–99%. Thus, plasma treatment to improve WHC alone is unnecessary for DES-FBPI. Higher gelling temperatures may affect its WHC and are worth exploring in future studies.

Based on previous studies, the WHC of DW-FBPI was expected to increase after PAW treatment. A study conducted by Dabade *et al.* (2023) demonstrated up to a 4.56% increase in WHC for pin-to-plate plasma treated soy protein isolate, citing exposure to reactive species from plasma treatment may have contributed towards increased hydrophilicity in the protein.[45]

As limited improvements in WHC were observed, it is concluded that PAW had no effects on hydrophilicity and WHC on FBPI gels. The unchanged WHC may limit juiciness in plant-based meat applications, but does not affect 3D printability (Section 3.13).

3.13 3D printability

The DW-FBPI gels for 3D printing were heated at 95, 85, and 80 °C. Gels that were heated at 95 °C were unfit for extrusion due to the hardness of the gel. Gels heated at 85 °C or lower were appropriate for 3D printing DW-FBPI. Higher gelling temperatures resulted in harder gels, which were more difficult to extrude (Fig. 5). Lower temperature gels resulted in smoother-looking 3D printed structures. This is demonstrated in structures E and F (Fig. 5).

Structures printed from 85 °C DW-FBPI gels were rough, uneven and lumpy. Gels prepared by heating at 80 °C for one hour produced the highest quality 3D printed structures. Treated samples prepared with PAW (B, D, F) generally produced higher quality and more accurate 3D printed structures (Fig. 5). Control samples produced inconsistent prints with brittle filaments. Brittle filaments are characterized by disconnected FBPI gel strands. As 3D printing is an additive manufacturing technique, deformed base layers contributed to
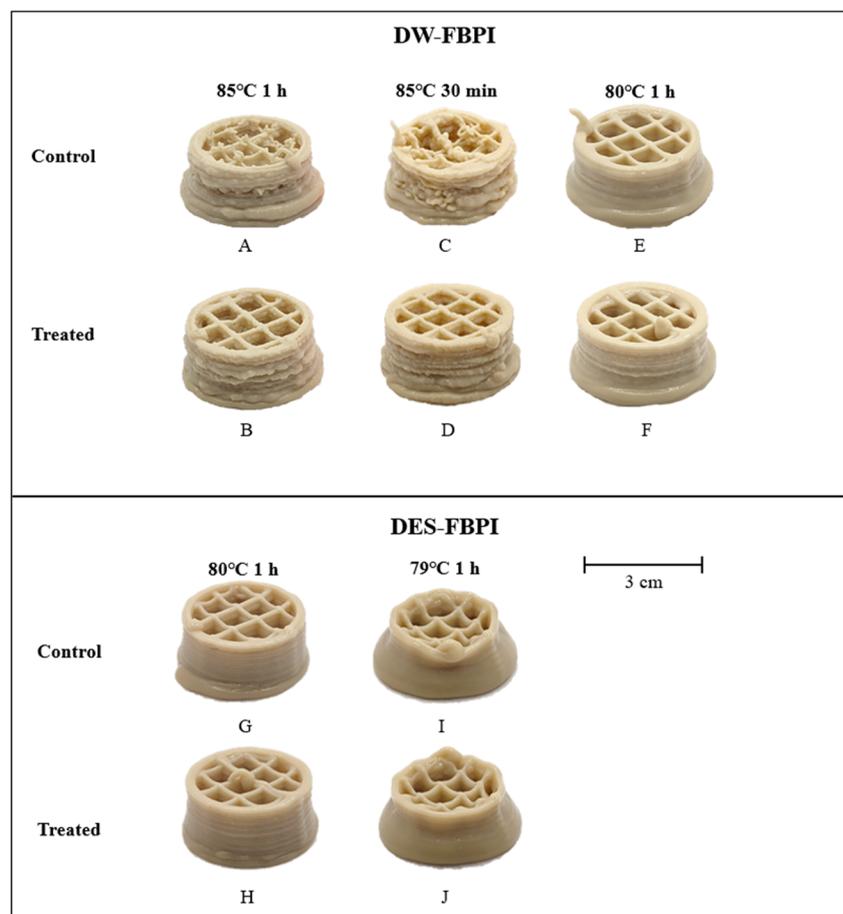

Fig. 5   3D printed structures of DW–FBPI and DES–FBPI gels.

deformed upper layers. In control samples, excess FBPI ink was dispensed, resulting in a brim forming around the shape. The degree of excess material extruded at the beginning of printing was not observed for treated 3D printed structures.

Significant differences were not observed in calculated ratios or digital measurements however, the data can be found in the supplementary data section. Effects of PAW in FBPI gels are visible through the quality of the prints opposed to measurements of the 3D printed structures themselves.

Treated DES-FBPI gels (Fig. 5) were heated at 79 °C and 80 °C; these specific temperatures were selected based on previous trials on the extrudability of the DES-FBPI gels. 3D printed structures created at 79 °C did not produce stable structures. Sagging and spreading were observed in both the control and treated samples. 3D printed gels created at 80 °C were structurally stable. Improved printing accuracy and resolution were also observed at this gelling temperature. The individual filaments were visible and aligned. For treated samples, 80 °C gelling conditions appeared to produce the best 3D printed structures. Differences between treated and control samples were challenging to differentiate based on visual observations; however, the treated sample H (Fig. 5) demonstrated less infill sagging compared to the control sample G (Fig. 5). This suggests the texture of sample H was modified and demonstrated better structural integrity. The β-sheet formation in DES-FBPI (Table 4) likely enhances gel network strength, improving filament integrity and reducing sagging.

Similar to the DW-FBPI, treated DES-FBPI did not produce significantly different numerical data on its shape and structure (Tables S8 and S9).

Due to the amount of variability in factors and printing conditions, comparison with pre-existing literature is challenging. Factors that affect 3D printability include shape design, material formulation, and 3D printing parameters. One paper studying the effects of PAW on pea proteins observed improvements in 3D printing; however, the modified variable was the difference in gases used for the creation of PAW.[5] To conclude, PAW treatment appears to positively affect the 3D printability of FBPI gels.

3.14 TPA

3.14.1 DW-FBPI – 30 min heating. A total of 4 conditions were examined for the TPA of DW-FBPI gels: treated and control samples heated at 95 °C and 85 °C. At a 30 min 95 °C–gelling temperature, the treated samples produced gels that were significantly softer ($P < 0.05$) than the control gels with approximately a 10.6% decrease in hardness (Table 5). At a 30 min gelling temperature of 85 °C, DW-FBPI treated gels were observed to be significantly more adhesive than the controls. Temperature was also observed to be a significant factor in the adhesiveness of the samples. Higher gelling temperatures resulted in lower adhesion, and *vice versa*. After running a 2-way ANOVA statistical test for adhesion, interaction between plasma treatment and temperature was present for gels heated at 85 °C for 30 min. This indicates that the temperature is significant in determining whether plasma treatment will significantly affect the adhesion of the samples.

The remaining parameters: springiness, gumminess, and cohesiveness had no significant differences ($P > 0.05$) with PAW treated DW-FBPI samples. However, temperature continues to be a significant factor in springiness and gumminess. DW-FBPI gels heated at 95 °C demonstrated higher springiness and gumminess compared to gels heated at 85 °C.

The physicochemical structure of a gel determines how it responds to external forces.[46] Parameters such as hardness and adhesion are dictated by the degree and types of cross-linkages present in a gel; therefore, changes in this parameter correspond to differences in gel structure. Significant changes in the TPA parameters suggest modification of the physicochemical structures of the gel. Interestingly, the effects of adding PAW in protein suspensions and subsequent gel preparations were not consistent with gelation temperatures. In terms of hardness, treated DW-FBPI gels heated at 95 °C demonstrated significant differences, whereas DW-FBPI gels heated at a lower temperature of 85 °C did not demonstrate any significant differences. This was also observed inversely with adhesion, where significant differences were only observed at a lower gelling temperature. This suggests that PAW in protein suspensions affected the TPA parameters of gels differently at different temperatures.

Table 5 Texture profile analysis data of DW-FBPI gels[a]

Gel temperature (°C)	Gel time	Treatment	Hardness (g)	Adhesiveness (g s)	Springiness (%)	Gumminess	Cohesiveness (%)
95	30 min	Control	1148.7 ± 88.6[a,A]	−58.5 ± 16.3[a,A]	83.0 ± 7.0[a,A]	366.87 ± 48.09[a,A]	32.0 ± 3.0[a,A]
	30 min	Treated	1027.3 ± 49.1[b,A]	−87.1 ± 38.6[a,A]	81.0 ± 9.0[a,A]	325.09 ± 42.42[a,A]	32.0 ± 4.0[a,A]
85	30 min	Control	417.3 ± 28.0[c,B]	−227.5 ± 108.9[b*,B]	67.0 ± 13.0[b,B]	126.3 ± 15.26[b,B]	30.0 ± 5.0[a,A]
	30 min	Treated	378.7 ± 74.9[c,B]	−454.1 ± 36.1[c*,B]	63.0 ± 3.0[b,B]	102.62 ± 16.68[b,B]	27.0 ± 2.0[a,A]
85	1 h	Control	525.6 ± 43.1[a,A]	−163.9 ± 36.9[a,A]	65.0 ± 3.0[a,A]	157.63 ± 21.71[a,A]	30.0 ± 2.0[a,A]
	1 h	Treated	534.8 ± 84.4[a,A]	−101.8 ± 33.9[a,A]	57.0 ± 16.0[a,A]	149.71 ± 31.62[a,A]	28.0 ± 3.0[a,A]
80	1 h	Control	172.5 ± 12.4[b,B]	−245.4 ± 26.6[b,B]	91.0 ± 3.0[b,B]	112.19 ± 20.20[a,A]	65.0 ± 7.0[b,B]
	1 h	Treated	221.5 ± 67.0[b,B]	−239.9 ± 14.2[b,B]	89.0 ± 4.0[b,B]	151.27 ± 60.14[a,A]	67.0 ± 6.0[b, B]

[a] Values are expressed as the mean ± the standard deviation of three replicates. 2-way ANOVA was completed with Tukey test as *post hoc* test. The first alphabetical superscript (a, b) within each columnar section indicates the values that are significantly different between control and treated within each temperature ($p < 0.05$). The presence of an asterisk (*) indicates interaction between plasma treatment and the respective TPA parameter. The second alphabetical superscript (A, B) indicates a significant difference in gel temperature ($p < 0.05$).

3.14.2 DW-FBPI – 1 h heating. DW-FBPI gels heated for 1 h at 85 °C and 80 °C demonstrated no significant differences after PAW treatment across all TPA parameters (Table 5). However, the gelling temperature did affect the hardness, adhesiveness, springiness, and cohesiveness of the gels. At 85 °C, the gel hardness was significantly higher than gels heated at 80 °C. In terms of adhesiveness, lower gelling temperatures resulted in higher adhesiveness in gels. Lower gelling temperatures also yielded gels with higher springiness. In terms of cohesiveness, gels heated at 80 °C also resulted in more cohesive gels. The gumminess of the gels remained unchanged regardless of treatment or change in gelling temperature. In general, the addition of PAW did not significantly affect any TPA parameters of DW-FBPI gels heated at 80 and 85 °C for one hour.

3.14.3 DES-FBPI. For DES-FBPI samples with a gelling temperature of 80 °C and 1 h of gelling time, no significant differences were observed between the PAW treated and control samples across all TPA parameters (Table 6). The 8 min treated DES-FBPI gels heated at 79 °C for one hour demonstrated a significant increase in hardness, adhesiveness, and cohesiveness. During trial phases, improvements in TPA parameters for treated samples were only observed at specific gelling temperatures. This was explored in the DES-FBPI samples, resulting in the selection of a 79 and 80 °C gelling temperature. At 80 °C, gels did not present any significant differences, whereas at 79 °C, significant differences were present. This suggests that the effect of the PAW mixing was only observable for gels heated at certain temperature ranges. The increased hardness and adhesiveness in DES-FBPI at 79 °C align with β-sheet formation observed through CD spectroscopy.

The results presented in Tables 5 and 6 are partly consistent with previous studies. In Menon *et al.* (2024) study on PAW treated pea protein, treated gels demonstrated an increase in hardness and adhesiveness.[5] Springiness and gumminess were not measured by Menon *et al.* (2024). No changes in cohesiveness for the PAW treated pea proteins were also recorded.[5] Based on these varied results, PAW treatments appear to effectively modify texture only at certain gelling temperatures with certain types of proteins. More exploration and condition optimization in gelling temperatures will aid in understanding the capabilities of PAW treatments on gel textures.

3.15 Rheology

Rheological data for the PAW treated FBPI gels are organized in sections based on similar gelling conditions for comparison.

Frequency sweeps (Fig. 6) are rheological oscillatory tests conducted at different frequencies with a constant amplitude specifically to explore the time-dependent deformation behavior in gel-like samples.[47] Frequency sweeps are conducted at specific strains as determined by amplitude tests and linear viscoelastic range (LVE). The LVE range is a region within the amplitude test in which the sample's stress is proportional to the strain.[47] According to Moreno *et al.* (2020), the minimal slope on the logarithmic coordinates of the G' and G'' allows the data to be fitted into a power law model.[48] Previous studies involving rheological data on food gels utilized the power law model to further extrapolate the rheological data.[5,48] Two equations are associated with the power law model:

$$G' = G'_0 \times \omega^{n'_0} \tag{9}$$

$$G'' = G''_0 \times \omega^{n''_0} \tag{10}$$

where G' (Pa) and G'' (Pa) represent the storage and loss modulus, respectively. G'_0 and G''_0 are the respective storage and loss modulus at ∼1 rad s^{-1} and finally, n'_0 and n''_0 are the exponents that represent frequency dependency of the storage and loss modulus.

3.15.1 DW-FBPI. All G' values were higher than G'' values (Fig. 6(A)), indicating gel-like characteristics. At the 95 °C–gelling temperature, treated samples had a higher G' than the control samples, signifying that the PAW mixing may have altered the gel rigidity and firmness. At a 95 °C gelling temperature, significant differences were observed for G'_0 and G''_0 between the treated and controlled samples (Table S6). The PAW treatment appears to increase both G' and G''. In addition, temperature also affects the parameters of the power law. Higher gelling temperatures yielded higher G'_0 values, indicating gel networks. Statistical analysis indicated no interaction within the data.

Table S6 and Fig. 6(B) represent DW-FBPI gels heated for one hour at 85 °C and 80 °C. Referring to Table S6, a significant difference was observed for gels heated at 85 °C for both the G'_0 and G''_0. Treated gels exhibited a higher G' signifying an increase in gel strength and rigidity. Higher G'_0 and G''_0 demonstrate higher resistance to deformation.[5] Gels heated at 80 °C did not exhibit any significant differences for both G'_0 and G''_0. Interestingly, in the 2-way ANOVA, interaction was detected for G'_0. This suggests that the changes in moduli (G'_0) are dependent on both temperature and PAW treatment, and the effect from one variable depends on the other variable. Significant differences were not observed in the n'_0 and n''_0 values.

Table 6 Texture profile parameters for DES-FBPI gels[a]

Treatment	Gelling conditions	Hardness (g)	Adhesiveness (g s)	Springiness (%)	Gumminess	Cohesiveness (%)
Treated – PAW 30 min	80 °C	233.5 ± 16.4[a]	−202.9 ± 63.3[a]	83.0 ± 6.0[a]	102.09 ± 17.07[a]	44.0 ± 6.0[a]
Control	80 °C	257.6 ± 44.4[a]	−235.6 ± 64.4[a]	81.0 ± 3.0[a]	101.17 ± 14.00[a]	40.0 ± 2.0[a]
Treated – PAW 8 min	79 °C	107.6 ± 6.7[a]	−146.5 ± 25.5[a]	81.0 ± 3.0[a]	48.63 ± 1.02[a]	45.0 ± 2.0[a]
Control	79 °C	63.3 ± 15.2[b]	−75.0 ± 15.5[b]	87.0 ± 2.0[a]	38.35 ± 8.40[a]	61.0 ± 5.0[b]

[a] Values are expressed as the mean ± the standard deviation of three replicates. 1-way ANOVA was completed with Tukey test as *post hoc* test. The alphabetical superscript (a, b) within each gel temperature indicates the values that are significantly different between control and treated ($p < 0.05$).
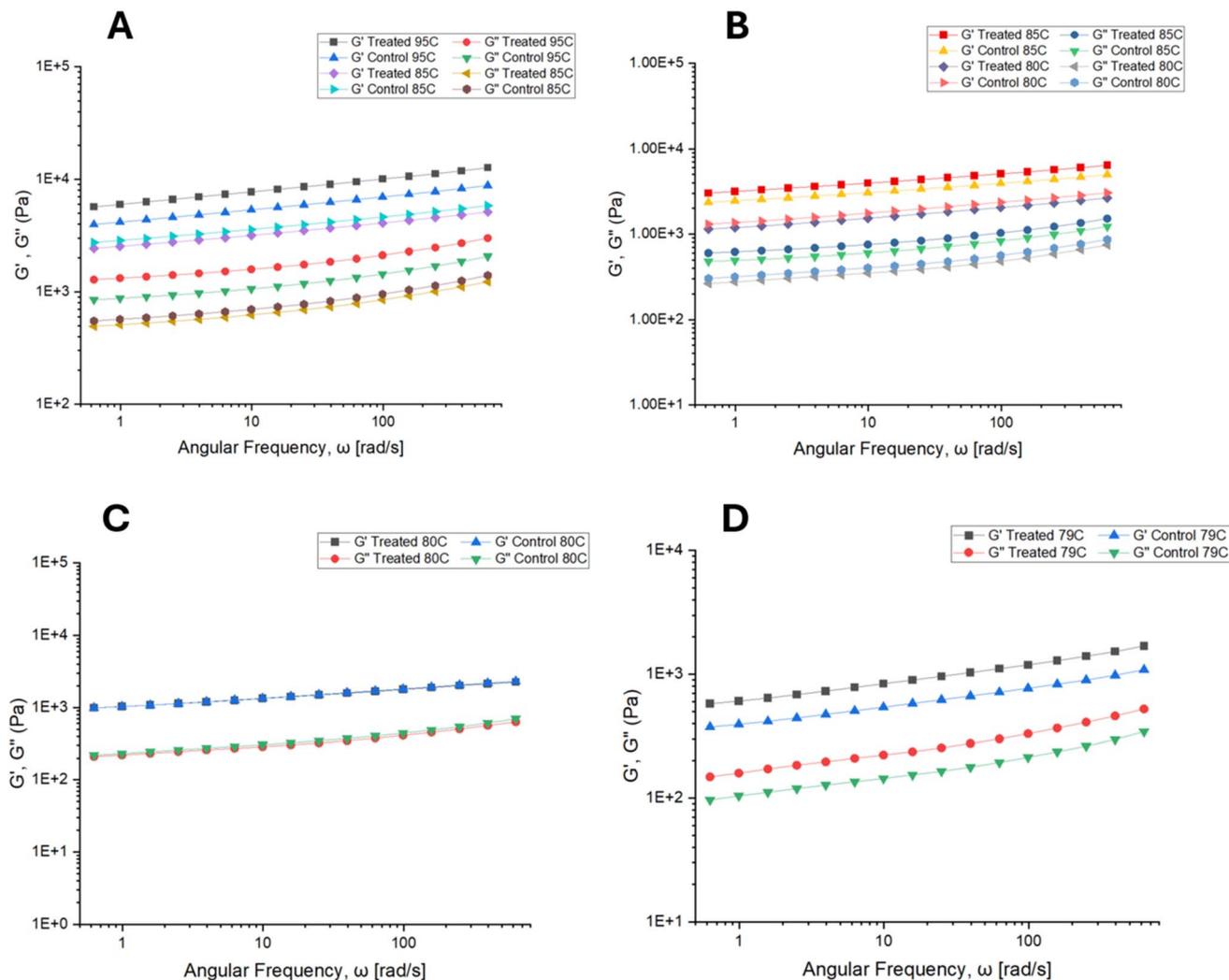
Fig. 6 Frequency sweep analysis of DW-FBPI and DES-FBPI. (A) Frequency sweep for DW-FBPI gels heated at 95 °C and 85 °C for 1 h. (B) Frequency sweep for DW-FBPI gels heated at 85 °C and 80 °C for 30 min. (C) Frequency sweep for DES-FBPI gels heated at 80 °C for 1 h. (D) Frequency sweep for DES-FBPI gels heated at 79 °C for 1 h with 8 min PAW.

3.15.2 DES-FBPI. At a gelling temperature of 80 °C, the treated DES-FBPI did not exhibit any significant differences compared to the control samples among all power law parameters. Referring to Fig. 6(C), treated and controlled data for G' and G'' are nearly superimposed, signifying that the PAW mixing did not result in any rheological property changes in the samples.

The last condition tested was gels formulated with 8 min PAW combined with protein suspension and gelled at 79 °C for one hour. The treated G' curve as well as the G'' curve is higher compared to the control curves (Fig. 6(D)). It is further supported by the data in Table S7 in which significant differences were observed for both G'_0 and G''_0. This suggests treated DES-FBPI gels increased in gel strength and resistance towards deformation. The G'_0 of the treated gels increased by approximately 56% compared to the control. Significant differences were also observed for the parameters n'_0 and n''_0. As mentioned previously, these exponential variables from eqn (4) and (5) represent the modulus' dependence on frequency. According to

Moreno *et al.* (2020)) $n' < n''$ indicates rate of decrease of G' is lower than the rate of decrease for G'' with decreasing angular frequency.[48] When the $n' < n''$ condition is fulfilled, the gels demonstrate higher gel-strength at lower frequencies indicating strong elastic gel structures. The increase in n' for the treated samples suggests that treated samples have higher gel strength and rigidity at lower frequencies compared to the control samples.

Overall, the results for the rheological data are mostly consistent with previous studies with PAW treated DW-FBPI and DES-FBPI demonstrating increased G' and G'' values compared to the control samples. The increased G' and G'' in treated gels indicate enhanced gel strength and rigidity, consistent with β-sheet formation (Table 4). In Menon *et al.*, (2024) study, pea protein gels treated with PAW demonstrated significantly higher G' and G'' values compared to the control sample gels, indicating increased gel strength.[5] This change indicates that the PAW treatment was successful in increasing the gel strength of the samples. However, there are several

anomalies such as DW-FBPI gels heated at 85 °C (30 min), 80 °C (1 h) and DES-FBPI gels heated at 80 °C (1 h) all of which did not demonstrate significant differences in G_0' and G_0'' values compared to the control. It is unclear why PAW isn't as effective for gels heated at these specific temperatures. Future studies investigating this anomaly is recommended.

4. Conclusions

Overall, the effects of combining PAW with FBPI were relatively effective in improving rheological properties and some of the texture profile parameters. In DW-FBPI and DES-FBPI, most treated samples demonstrated improved gel strength and increased resistance against deformation. Based on the CD analysis data, PAW treatment was very effective in reducing helical structures and increasing beta sheets, which may have led to the enhanced gel-strength and improved 3D printability, as β-sheets promote intermolecular interactions critical for gel networks. In addition, treated samples demonstrated improved 3D printability compared to control samples. The work completed in this study highlights the feasibility of modifying FBPI using PAW; however, additional work is needed to determine the effect of specific parameters such as voltage, frequency and treatment times of PAW generation on specific protein functionality. Some functionalities that were unaffected by the PAW treatment include viscosity, solubility and WHC, all of which are crucial in food production applications. This may indicate that PAW treatment requires more intensive conditions to induce significant changes in these properties. In addition, it is important to explore optimized PAW treatment times, as 8 min PAW treatment was just as efficient in inducing rheological improvements in DES-FBPI compared to 30 min PAW treatments. Future studies can focus on further developing and optimizing PAW treatments for targeted applications in the food industry.

Conflicts of interest

The authors declare no conflict of interest.

Abbreviations

DES-FBPI	Deep eutectic solvent extracted fava bean protein isolates
DW-FBPI	Dry and wet extracted fava bean protein isolates
FBPI	Fava bean proteins isolates
DES	Deep eutectic solvent
PAW	Plasma activated water
OES	Optical emission spectroscopy
FTIR	Fourier transform infrared spectroscopy
CD	Circular dichroism
WHC	Water holding capacity
LVE	Linear viscoelastic range

Data availability

Data is available on request.

Supplementary information is available. See DOI: https://doi.org/10.1039/d5fb00481k.

References

1 C. Saldanha do Carmo, S. H. Knutsen, G. Malizia, T. Dessev, A. Geny, H. Zobel, K. S. Myhrer, P. Varela and S. Sahlstrøm, *Future Foods*, 2021, **3**, 100014.
2 L. Day, J. A. Cakebread and S. M. Loveday, *Trends Food Sci. Technol.*, 2022, **119**, 428–442.
3 W. Kim, Y. Wang and C. Selomulya, *Trends Food Sci. Technol.*, 2020, **105**, 261–272.
4 N. N. Misra, T. Naladala and K. J. Alzahrani, *J. Phys. D: Appl. Phys.*, 2024, **57**, 493003.
5 S. C. Menon, H. K. Dhaliwal, L. Du, S. Zhang, J. Wolodko, L. Chen L and M. S. Roopesh, *Food Biosci.*, 2024, **59**, 104050.
6 S. Zhang, W. Huang, E. Feizollahi, M. S. Roopesh and L. Chen, *Food Sci. Emerging Technol.*, 2021, **67**, 102567.
7 S. Zhang, W. Huang, M. S. Roopesh and L. Chen, *Food Res. Int.*, 2022, **154**, 111028.
8 J. Li, W. Rao, Y. Sun, C. Zhou, Q. Xia, J. He, D. Pan and L. Du, *Food Res. Int.*, 2024, **197**, 115271.
9 T. Asledottir, G. E. Vegarud, G. Picariello, . Mamone, T. E. Lea, A. Røseth, P. Ferantti and T. Devold, *J. Funct. Foods*, 2023, **102**, 105445.
10 T. Vasanthan. *US Pat.*, US20170087596A1, 2017.
11 B. Jeganathan, J. Gao, F. Temelli and T. Vasanthan, *J. Food Eng.*, 2023, **339**, 111265.
12 A. Hewage, O. O. Olatunde, C. Nimalaratne, J. D. House, R. E. Aluko and N. Bandara, *Food Hydrocolloids*, 2024, **147**, 109283.
13 D. B. Jones, *Factors for Converting Percentages of Nitrogen in Foods and Feeds into Percentages of Protein*, US Department of Agriculture, 1941, vol. 183, p. 22.
14 F. Mariotti, D. Tomé and P. P. Mirand, *Crit. Rev. Food Sci. Nutr.*, 2008, **48**, 177–184.
15 2015 Malvern Instruments Limited, Zeta potential - An introduction in 30 minutes. https://www.research.colostate.edu/wp-content/uploads/2018/11/ZetaPotential-Introduction-in-30min-Malvern.pdf, accessed January 2025.
16 F. Yang, C. Guo, M. Zhang, B. Bhandari and Y. Liu, *LWT – Food Sci. Technol.*, 2019, **102**, 89–99.
17 A. Rodger and D. Marshall, *Biochemist*, 2021, **43**, 58–64.
18 A. Kramida, Y. Ralchenko, J. Reader and NIST ASD Team, *NIST Atomic Spectra Database (Version 5.12)*, National

Institute of Standards and Technology, Gaithersburg, MD, 2024, Available from: https://physics.nist.gov/asd, Accessed Mar 30 2025.

19 R. Zhou, R. Zhou, K. Prasad, Z. Fang, R. Speight, K. Bazaka and K. Ostrikov, *Green Chem.*, 2018, **20**, 5276–5284.

20 H. M. Roomy, A. N. Yasoob and H. H. Murbat, *Kuwait J. Sci.*, 2023, **50**, 163–167.

21 N. Giannakaris, G. Gürtler, T. Stehrer, M. Mair and J. D. Pedarnig, *Spectrochim. Acta, Part B*, 2023, **207**, 106736.

22 Q. Luo, W. Zhan, R. M. Boom and A. E. M. Janssen, *Food Funct.*, 2018, **9**, 5283–5289.

23 S. Perinban, V. Orsat and V. Raghavan, *Int. J. Food Sci. Technol.*, 2023, **58**, 1346–1355.

24 H. Ji, S. Dong, F. Han, Y. Li, G. Chen, L. Li and Y. Chen, *Food Bioprocess Technol.*, 2018, **11**, 344–354.

25 O. O. Alabi, G. A. Annor and E. O. Amonsou, *Food Struct.*, 2023, **36**, 100321.

26 F. Sun, X. Xie, Y. Zhang, M. Ma, Y. Wang, J. Duan, X. Lu, G. Yang and G. He, *Food Biosci.*, 2021, **39**, 100808.

27 G. Chen, S. Dong, Y. Chen, Y. Gao, Z. Zhang, S. Li and Y. Chen, *Food Hydrocolloids*, 2020, **107**, 105943.

28 R. Laurita, D. Barbieri, M. Gherardi, V. Colombo and P. Lukes, *Clin. Plasma Med.*, 2015, **3**, 53–61.

29 S. Chen, A. E. Hall and C. I. Moraru, *J. Food Sci.*, 2023, **88**, 4630–4638.

30 G. Chen, R. A. Barron and M. V. P. Raja, in *Physical Methods in Chemistry and Nano Science,* ed. Barron R. A. and Raja M. V. P., Midas Green Innovations, Ltd, 2019. pp. 187–193.

31 J. M. Berg, A. Romoser, N. Banerjee, R. Zebda and C. M. Sayes, *Nanotoxicology*, 2009, **3**, 276–283.

32 Q. Wang, C. Gu, R. Wei, Y. Luan, R. Liu, Q. Ge, H. Yu and M. Wu, *Ultrason. Sonochem.*, 2023, **94**, 106349.

33 N. J. Greenfield, *Nat. Protoc.*, 2006, **1**, 2876–2890.

34 H. Sharafodin and N. Soltanizadeh, *Food Hydrocolloids*, 2022, **122**, 107077.

35 C. H. Wang and S. Damodaran, *J. Agric. Food Chem.*, 1991, **39**, 433–438.

36 Y. Ji, X. Yang, Z. Ji, L. Zhu, N. Ma, D. Chen, X. Jia, J. Tang and Y. Cao, *ACS Omega*, 2020, **5**, 8572–8578.

37 M. Palencia, *J. Adv. Res.*, 2018, **14**, 53–62.

38 J. Andrade, C. G. Pereira, J. C. Almeida, C. C. R. Viana, L. N. Neves, P. H. F. Silva, M. Bell and V. Anjos, *LWT*, 2019, **99**, 166–172.

39 N. Bahrami, D. Bayliss, G. Chope, S. Penson, T. Perehinec and I. D. Fisk, *Food Chem.*, 2016, **202**, 247–253.

40 F. E. O'Kane, J. M. Vereijken, H. Gruppen and M. A. J. S. Boekel, *J. Food Sci.*, 2005, **70**, 132–137.

41 S. Bandyopadhyay and A. Dey, Convenient detection of the thiol functional group using H/D isotope sensitive Raman spectroscopy, *Analyst*, 2014, **139**, 2118–2121.

42 J. P. Farr, W. L. Smith and D. S. Steichen, Kirk-Othmer Encyclopedia of Chemical Technology, 2003, https://onlinelibrary.wiley.com/doi/full/10.1002/0471238961.1921182206011818.a01.pub2, accessed 2025 Jul 8.

43 M. H. Mahdavian and A. Koocheki, *Food Hydrocolloids*, 2023, **143**, 108846.

44 S. Bußler, V. Steins, J. Ehlbeck and O. Schlüter, *J. Food Eng.*, 2015, **167**, 166–174.

45 A. Dabade, S. Kahar, A. Acharjee, P. Bhushette and U. Annapure, *J. Agric. Food Res.*, 2023, **12**, 100538.

46 A. M. Grillet, N. B. Wyatt, L. M. Gloe, in *Rheology*, 2012. vol. 3, pp. 59–80.

47 T. G. Mezger, in *The Rheology Handbook for Users of Rotational and Oscillatory Rheometers*, European Coatings Library, Hanover, Germany, vol. 4, 2014.

48 H. M. Moreno, F. Domínguez-Timón, M. T. Díaz, M. M. Pedrosa, A. J. Borderías and C. A. Tovar, *Food Hydrocolloids*, 2020, **99**, 105375.